ADVANCED FUNCTIONAL MATERIALS
www.afm-journal.de

Reversible Attachment with Tailored Permeability: The Feather Vane and Bioinspired Designs

*Tarah N. Sullivan, Michael Chon, Rajaprakash Ramachandramoorthy, Michael R. Roenbeck, Tzu-Tying Hung, Horacio D. Espinosa, and Marc A. Meyers**

In bird flight, the majority of the wing surface consists of highly refined and hierarchically organized feathers. They are composed of barbs that stem from the feather shaft and barbules that branch from barbs, forming a rigid feather vane. Barbules provide adhesion within the vane through an interlocking hook-and-groove mechanism to allow for the effective capture of air. This functional adhesive can reattach if structures unfasten from one another, preventing catastrophic damage of the vane. Here, using pelican primary feathers as a model material, we investigate the in-plane adhesion and stiffness of barbules. With guineafowl, pelican, and dove feathers, we determine the effect of barbules on the feather vane's ability to capture air. The vane is found to have directional permeability, and the effect of detaching barbules on the feather's competency is determined to be a function of barb dimensions. Interestingly, barbule spacing is found to vary within a narrow 8–16 µm range for birds weighing from 4–11 000 g (hummingbird to condor). Additionally, bioinspired barbules are fabricated through additive manufacturing to study the complexities of the vane. Barbules are underexplored structures imperative to the adeptness of the feather in flight, with the potential to provide bioinspired aerospace materials.

1. Introduction

Feathers are an essential evolutionary achievement for bird flight; their intricate design sustains lift with lightweight efficiency.[1] Flight feathers, composed entirely of β-keratin, have an architecture consisting of a main shaft (rachis and calamus), and a vane in which barbs branch from the rachis and barbules branch from barbs[2,3] (**Figure 1**a). Rigid barbs serve as the vane's backbone, while barbules interlock, resulting in cohesion of the vane[4] (**Figure 2**c). On a given barb, proximal barbules are grooved, while distal barbules have microhooks (hooklets) at their ends, adhering adjacent barbs[5,6] (Figure 1b–e).

The sophisticated architecture of barbule adhesion evolved during the Late Jurassic period with the advancement of aerial locomotion.[9] These structures are capable of detaching (unzipping) and reattaching, thus preventing irreversible damage to the entire vane[10] (Figure 2b; Video S1 in the Supporting Information). The barbule is considered a fundamental element for bird flight because it allows the feather vane to capture air effectively, mitigates irremediable damage by permitting localized failure, and enables the repair of damaged areas through preening.[11–13] For these reasons, feathers are an advantageous material for the bird wing as opposed to a continuous structure, such as the bat's skin flaps (patagium) (Figure 2a).

Despite the importance of barbules to bird flight, they have been largely neglected from research, possibly due to their microscale dimensions. Kovalev et al.[10] investigated the separation force of hooklets in swan (*Cygnus olor*) feathers and found they typically collectively separate at ≈0.27 mN. Additionally, despite a lack of experimental inquiry, many researchers assume that flight feathers are impervious to air[6,14] due the membranous flaps of barbules (Figure 1c) that overlap. A few published experiments report vaguely that there is a difference in feather transmissivity of 10–1000%[15,16] between the dorsal and ventral direction, due to barbules that act as one-way valves (V. Lougheed is cited by Raspet, 1960). While these works are fundamental to understanding barbule adhesion and vane permeability, there is ample room for investigation.

Here, we examine three aspects of the barbule, essential to the vane's function: 1) its adhesive properties, 2) stiffness, and 3) ability to capture air. We demonstrate that these three facets of barbules allow the feather vane to be a versatile material capable of maintaining lift while remaining flexible, and provide insight into specific features of barbules that are of high relevance to the feather's efficiency. Research in this area has the potential to lead to the fabrication of bioinspired control surfaces for enhanced performance of aerospace materials.

T. N. Sullivan, T.-T. Hung, Prof. M. A. Meyers
Department of Mechanical and Aerospace Engineering
University of California
San Diego, La Jolla, CA, USA 92093
E-mail: mameyers@eng.ucsd.edu
Dr. M. Chon, R. Ramachandramoorthy, M. R. Roenbeck, Prof. H. D. Espinosa
Department of Mechanical Engineering
Theoretical and Applied Mechanics Program
Northwestern University
Evanston 60062, IL, USA

DOI: 10.1002/adfm.201702954

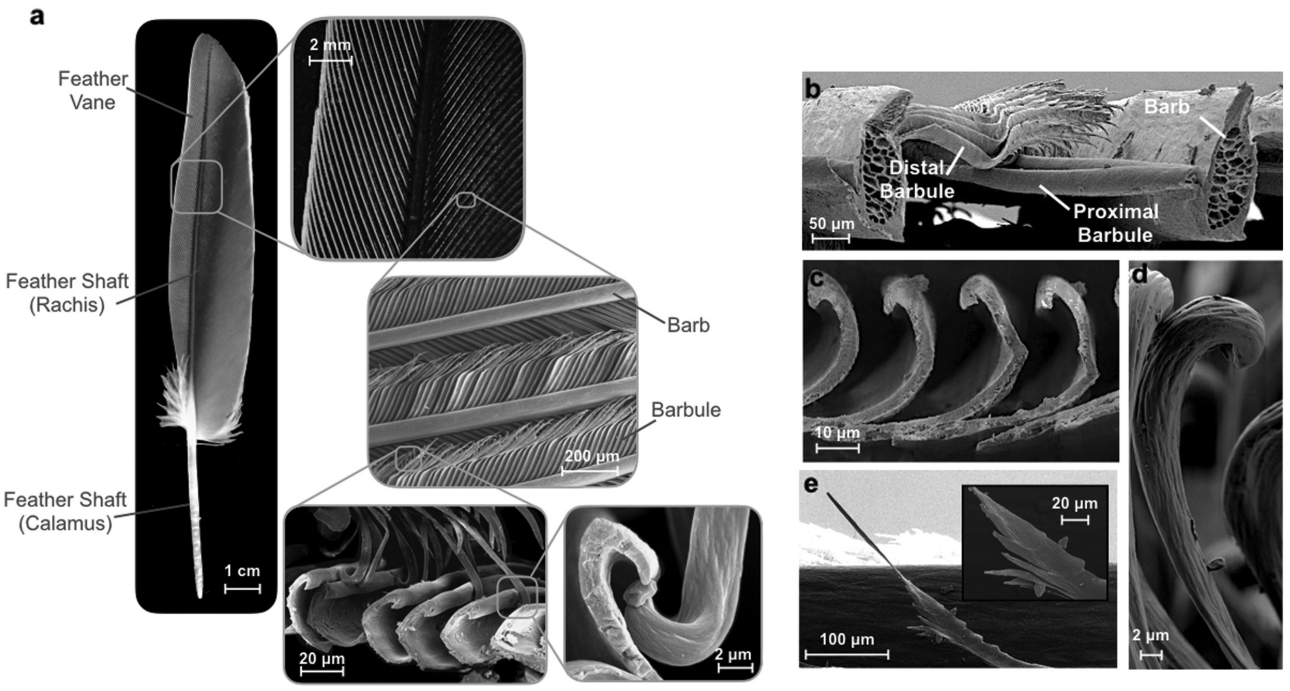

Figure 1. a) Flight feathers are composed of a main shaft (rachis and calamus), barbs that branch from the rachis and barbules that stem from barbs. Reproduced with permission.[7] Copyright 2017, Elsevier. b) Hooked, distal barbules branch from the left barb to interlock with the neighboring barb's grooved, proximal barbules. This allows neighboring barbs to adhere to one another and form a tightly woven material that traps air. c) Grooved barbules are sliced to reveal their cross-sections. d) Microhooks (hooklets), such as the one pictured here, occur at the end of hooked barbules. e) In most bird species there are ridges at the ends of grooved barbules, possibly to increase friction.

2. Results and Discussion

2.1. Adhesion within the Feather Vane

Adhesion within the pelican feather vane is investigated by applying in-plane tension to "unzip" a rectangular section of the vane separated from the shaft. Prior to failure, barbules maintain adhesion as barbs rotate uniformly in the proximal direction (**Figure 3**b). This is likely due to the geometric differences between grooved and hooked barbules; grooved barbules branch from barbs at a smaller angle ($\alpha = 17.9 \pm 2.0°$, $\beta = 41.8 \pm 2.3°$) and have a longer length ($L_g = 603.2 \pm 8.6$ µm, $L_h = 409.1 \pm 20.8$ µm) resulting in a greater applied moment and subsequent proximal rotation (Figure 3a; calculations in Section S1 in the Supporting Information). When connected to the shaft, however, the vane prefers to rotate distally due to the angle at which barbs branch from the rachis.[17] This difference in rotational preference between the hierarchical levels of the feather is thought to help maintain the area of the vane; if both barbs and barbules favored distal rotation, the vane would easily collapse. Similar geometric differences between hooked and grooved barbules are evident in many other flying birds such as the guineafowl and the dove, indicating that the attachment behavior witnessed here is not specific to the pelican feather.

As barbs rotate, hooks of distal barbules slide along the grooves of proximal barbules and then rapidly unhook and detach in brittle-like separation (Figure 3c). The experimentally determined work is normalized for a single hook connection ($W_{hook} = 1.58 \times 10^{-9}$ Nm) and compared to the calculated energy of separation of a pelican hook ($E_{hook} = 1.42 \times 10^{-9}$ Nm) based on dimensions measured from scanning electron microscope images (calculations in Section S2 in the Supporting Information). The similarity of these values validates the method of testing, since the energy of separation for a single hook can be equated to its work by the first law of thermodynamics. Calculations greatly simplify the complex detachment of barbules into an intelligible process and demonstrate the fidelity of this testing method.

2.2. Interlocking Bioinspired Hooks and Grooves

Arguably the most important aspect of barbule adhesion is the interlocking hook-and-groove mechanism. Adhesion experiments with 3D-printed grooves and various bioinspired hooks elucidate important features of hook design in the vane through simplification and scaling-up. Bioinspired barbules are composed of material with a considerably lower elastic modulus (NinjaFlex filament, elastic modulus = 12 MPa, see Section S7 in the Supporting Informationfor details) than the feather to compensate for their significantly larger dimensions, providing a similar stiffness and comparable adhesion characteristics to the feather. The hook thickness, shape, and wrap at the end of the hook were investigated as aspects influencing adhesion. Hooks A–C are thicker at the base of the hook (4 mm) than hooks D and E (2.2 mm), and hooks A,C,D have a rectangular hook shape, while hooks B and E have a circular hook shape.

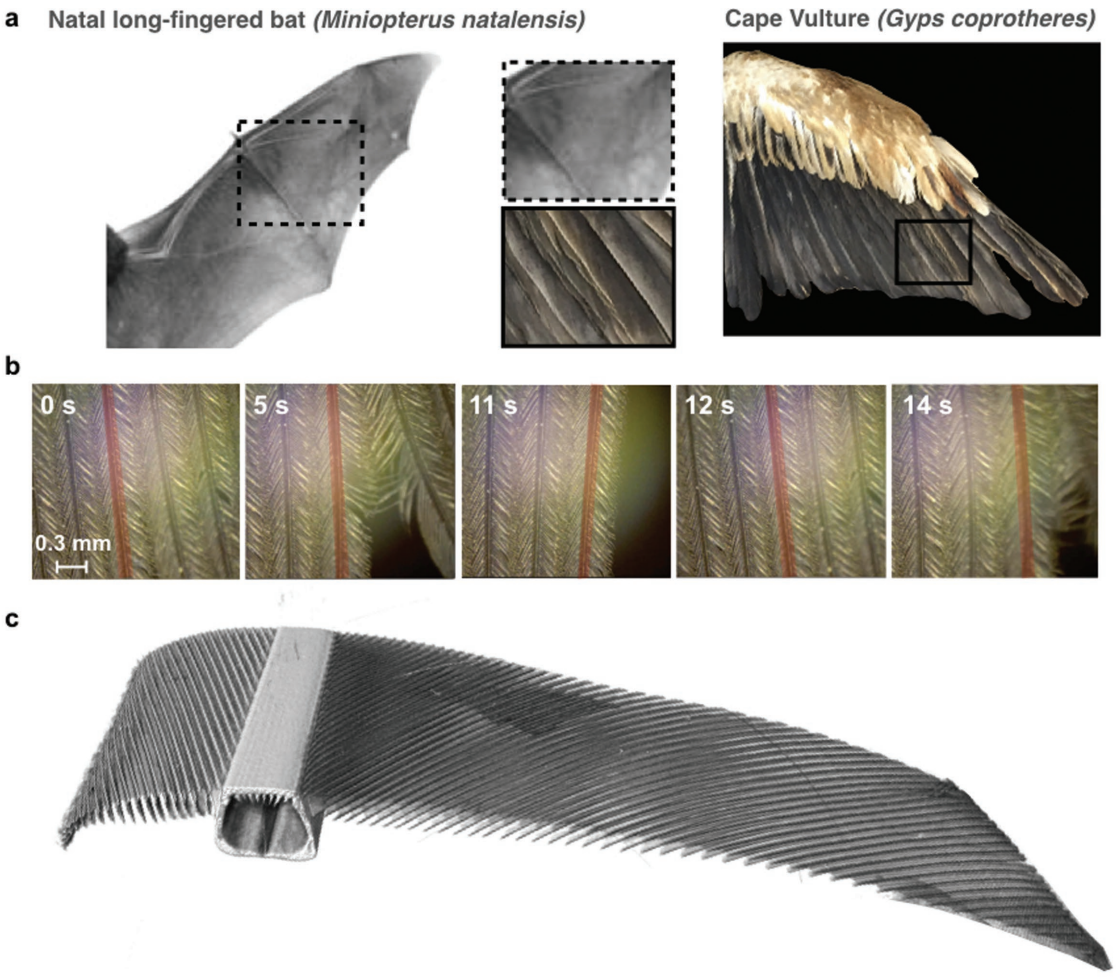

Figure 2. a) Bat's wings are composed of continuous skin flaps (patagium) while the complex feathers of birds allow for localized failure. Adapted with permission.[8] Copyright 2016, Springer Nature. b) One of the advantages of the feather vane is that it can be separated and reattached; images of the feather vane taken at various moments during unzipping and rezipping. The vane begins in tact (0 s), then begins to unzip (5 s), becomes completely detached (11 s), is released and returns back to its original position (12 s), and is unzipped again (14 s). A barb is highlighted in red to mark its position throughout the various frames. c) A microcomputerized tomography (μ-CT) generated image of an Andean Condor (*V. gryphus*) feather shows the cohesion of the vane. Reproduced with permission.[7] Copyright 2017, Elsevier.

Finally, C has a shorter hook tip and therefore wraps around grooves less than the other hooks.

As one of the thicker hooks created, hook A has the highest maximum adhesion force, effectively wrapping around the groove structure with a rectangular-shaped hook (Figure 3d,e). Readhesion experiments, measured by the percent of maximum force recovered in cyclical tests without manually interlocking hooks, reveal that hooks D and E readhere best while hook B readheres worst (Figure 3f). The flexibility of hooks D and E (due to their thin structure) allow them to easily bend around grooves and reattach when displaced back to their original position. Hook E, however, has less total hook length than hook D, resulting in a smaller displacement at its maximum force. The increased curvature of hook B serves as an obstacle for readhesion, though it provides a tight-fitting connection to the groove for interlocking adhesion. In these experiments it was found that a rectangular hook shape provides more strength for interlocking attachment than a circular hook shape,[18] thinner hooks allow for enhanced recovery of attachment, and a wrapped hook tip (as compared between A and C) increases the maximum force but does not significantly influence readhesion. Both experiments demonstrate the importance of the hook shape on two necessary functions of the vane: adhesion and the ability to re-adhere. Hooks evolved to strike an optimum balance between these two functions with seemingly contrasting requirements.

2.3. Barbule Flexure

Since barbules are the least rigid component of the feather vane, their stiffness is an integral part of the vane's critical "unzipping" mechanism. A method for measuring the stiffness of barbules is developed through in situ scanning electron

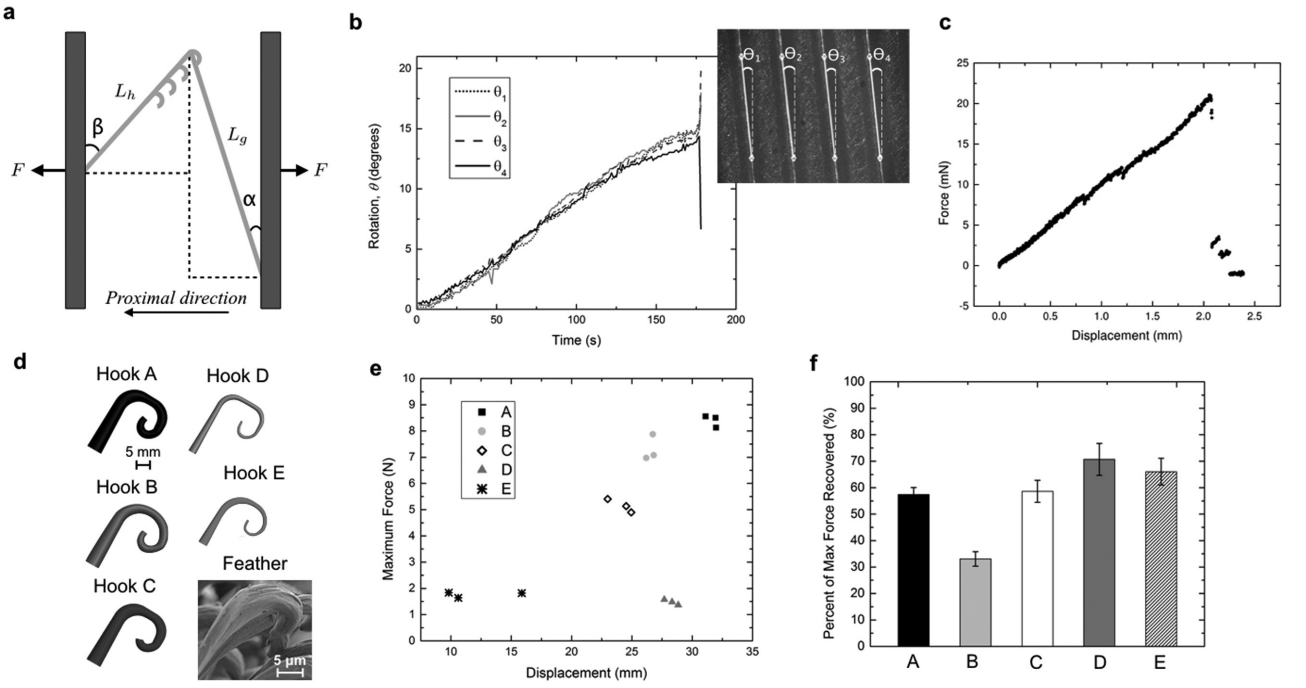

Figure 3. In-plane tension tests of the pelican feather vane: a) A schematic of the lengths and angles of the hooked barbule (L_h, β) and grooved barbule (L_g, α) demonstrating the greater moment applied to grooved barbules and resulting proximal rotation. b) Before failure, barbules maintain attachment as barbs rotate proximally at angle theta (θ) throughout the test. This angle is shown in the optical microscope image (right) where dashed lines mark the original position of the barbs, and the solid white lines trace the ending position of barbs. c) An example plot of the measured force versus displacement reveals that on the macroscale pelican feathers exhibit brittle-like failure when unzipped. Adhesion of bioinspired hook and groove structures: d) Hooks A–E were created through 3D printing. e) The maximum force versus displacement for tension tests of the hook and groove structures reveals that hook A has the maximum force of adhesion. f) Hooks D and E were found to have the highest percent of maximum force recovered in re-adhesion tests. The same set of grooves were used for all adhesion tests.

microscopy (SEM) experiments in which an atomic force microscopy (AFM) tip connected to a nanomanipulator displaces a single barbule (Figure 6c). Critical snapshots from in situ SEM experiments are shown in **Figure 4**a. The flexural stiffness of a single hooked pelican barbule was experimentally measured to be 0.061 N m^{-1}, while its calculated value is determined to be 0.048 N m^{-1} using a highly simplified analytical model with dimensions measured from SEM images (see Section S3 in the Supporting Information for detailed information). Since these two estimates are within a reasonable range of one another (≈20%), the viability of this method is confirmed. Although the stiffness measured in this experiment is specific to a hooked pelican barbule (since barbule length[7] and cross section vary among birds) the results can be used to determine an order of magnitude of barbule stiffness for these structures, as this is the first time barbule stiffness has been measured.

In flight, forces due to airflow cause barbules to first deflect and then slide along one another until they rapidly detach. It is hypothesized, therefore, that a stiffer barbule will allow the vane to handle larger out-of-plane forces before unzipping. This in turn would increase the vane's capacity for loading before local failure, and thus impact the maximum force the vane could sustain in flight. Barbule stiffness can be used in conjunction with future work to relate the in-plane adhesive properties to the out-of-plane forces of flight.

2.4. Barbule Adhesion and the Feather's Ability to Capture Air

The significance of barbule adhesion to the feather's ability to capture air is measured in wind tunnel experiments. In these tests, the drag force is compared between intact feathers and unzipped feathers, where barbules are disengaged. Experimental details are explained later in the paper (Figure 6d). Experiments reveal that the drag force of the feather decreases as the percentage of unzipped barbs within the vane increases. This effect is magnified at higher airspeeds (Figure 4b,c). The drag force[19]

$$F_{\text{drag}} = \frac{1}{2}\rho u^2 c_{\text{D}} A \tag{1}$$

is comprised of several factors: ρ is air density, u is the speed of the feather relative to the air, C_{D} is the drag coefficient of the feather, and A is the orthographic projected area of the vane onto a plane perpendicular to the flow. Due to its flexible nature, as air velocity increases the force on the feather vane causes barbs to deflect away from airflow. When deflected to an extreme the projected area of the vane *(A)* becomes smaller than its original size, subsequently decreasing the drag force (F_{drag}). Since unzipped barbs are less restricted in movement,[20] this deflection occurs at a lower velocity for unzipped barbs than zipped barbs. In these experiments, a larger drag

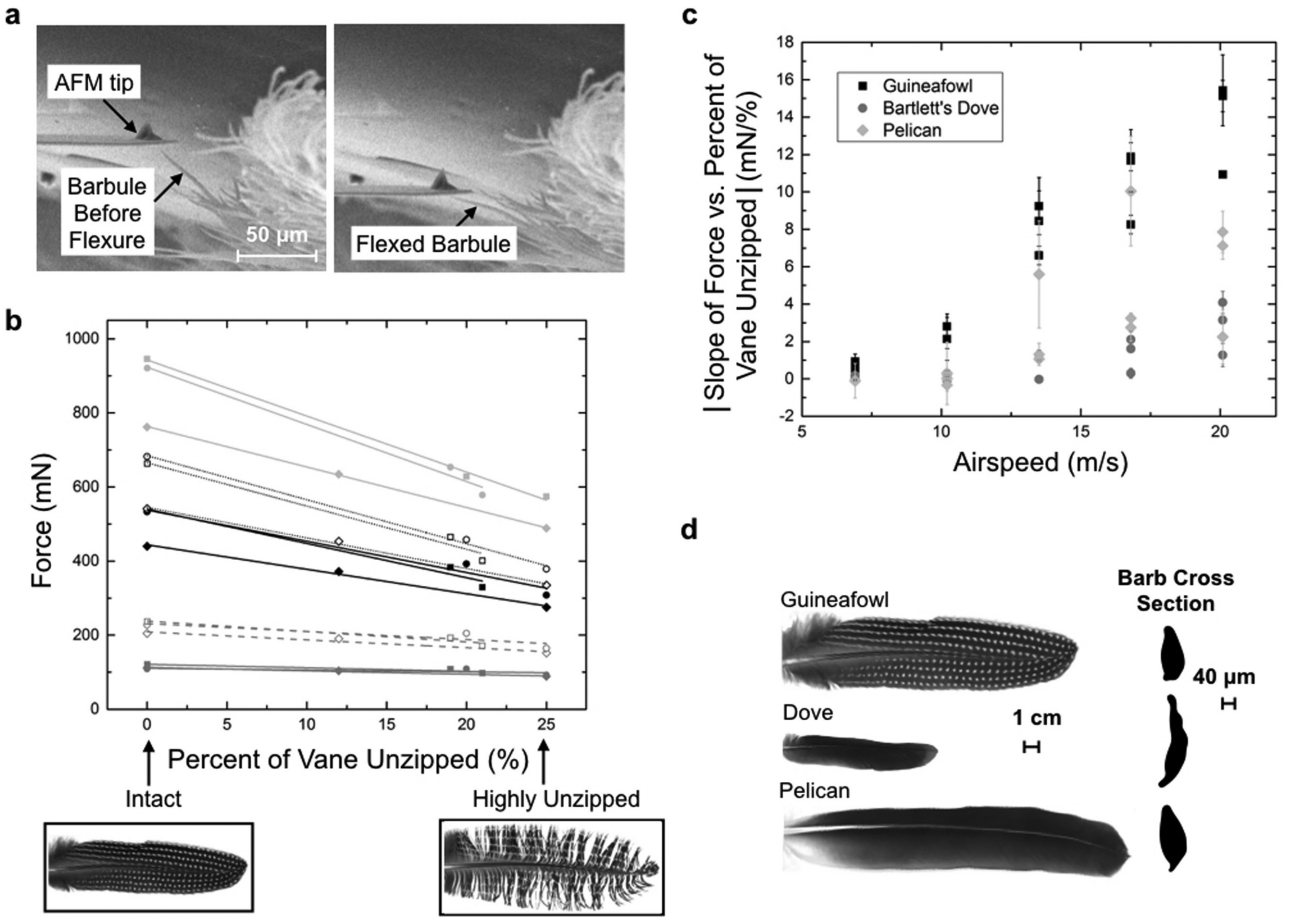

Figure 4. a) Critical snapshots of the barbule during in situ SEM flexure experiments: (left) at the initial position immediately before contact, (right) at the maximum load, just before separation. b) Force versus percent of the vane unzipped for the guineafowl feather. Different line types correspond to the airspeed feathers were tested at: solid gray is 6.91 m s^{-1}, dashed gray set is 10.20 m s^{-1}, solid black is 13.50 m s^{-1}, dotted black set is 16.80 m s^{-1}, and solid light gray is 20.09 m s^{-1}. Images are examples of the guineafowl feather intact and highly unzipped. c) The absolute value of the slope of force versus percent of vane unzipped is plotted against airspeed. The guineafowl consistently has the highest slope, meaning that it is most effected by unzipping. d) Dimensions of each species' feather barbs relate to the effect of unzipping.

force corresponds to a vane that is able to capture air more effectively.

While feathers from all three birds studied here (dove, pelican, and guineafowl) demonstrate a decrease in drag force with an increase in percent of unzipped barbs, each exhibits this at a different magnitude. Figure 4c displays the absolute value of the slope of force versus the percent of vane unzipped. The guineafowl feather consistently has the highest slope value, meaning that it is most dramatically effected by unzipping, while the dove feather has the lowest slope value, being the least effected by unzipping. This is again related to the drag equation: the guineafowl has long, narrow barbs (Figure 4d) that deflect relatively easier, reducing the vane's drag force to a greater extent than the other species' feathers (see Section S4 in the Supporting Information for statistical analysis). The dove feather however, has thicker, stiffer barbs (Figure 4d) making deflection difficult and therefore maintaining a similar projected area whether or not the vane is unzipped. Perhaps this is an evolutionary reflection of the flight style of each bird; both the dove and pelican rely on flight as their primary mode of locomotion, whereas guineafowl mainly run with only occasional flight. Consequentially, a reduction in ability to capture air would arguably be more detrimental to the dove and pelican's survival than the guineafowl.

2.5. Directional Permeability of the Feather Vane

Not only do barbules provide adhesion to allow barbs to trap air effectively, they are hypothesized to capture air via thin, overlapping, membranous side flaps. These flaps (**Figure 5**a) appear as one-way valves, impermeable to air flow in the ventral direction but not in the dorsal direction. An additively manufactured model conceptually demonstrates this in Figure 5b,c: with dorsal airflow the flaps open and with ventral airflow flaps remain closed.

The difference in permeability of the feather with ventral and dorsal airflow is measured by sealing barbule membrane flaps shut with a coating, and comparing the uncoated and

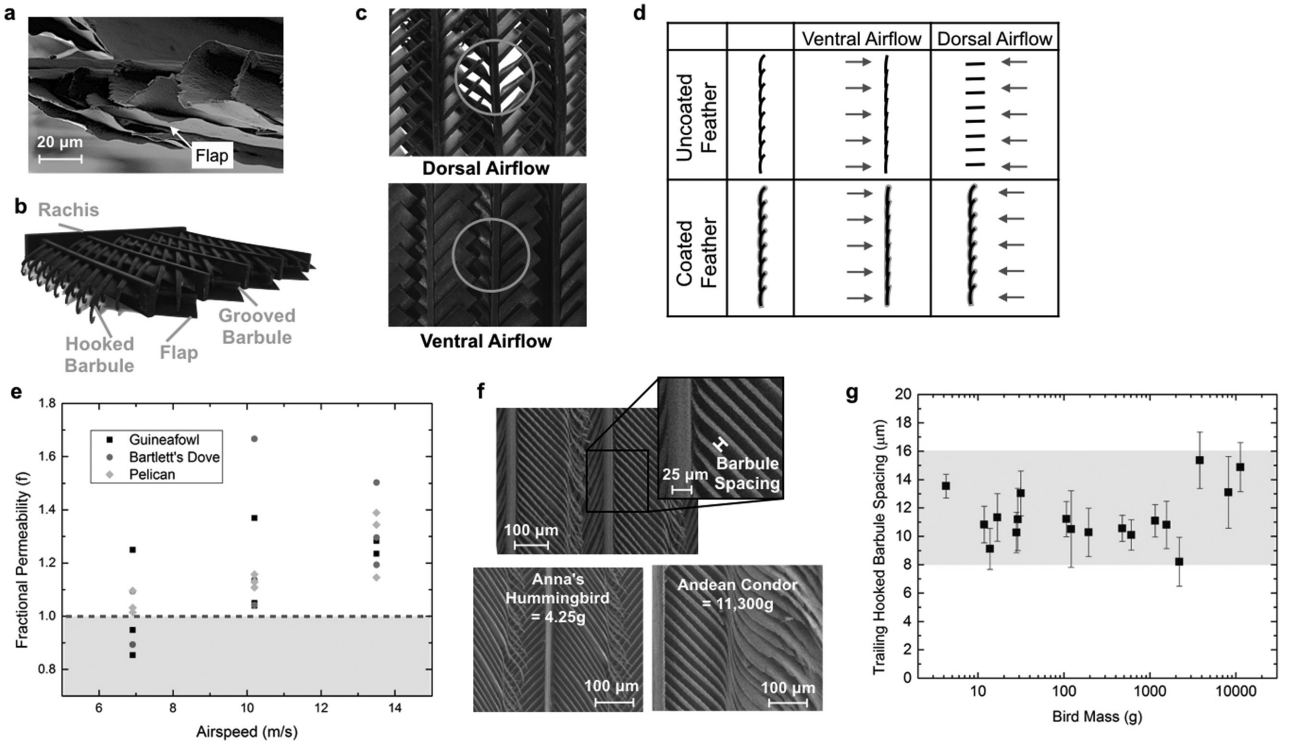

Figure 5. a) An arrow points to an example of a barbule membrane. b) A simplified, 3D-printed model of the feather vane, and c) the hypothesized reaction of membrane flaps as air is blown dorsally (top) and ventrally (bottom), where circles represent the location of airflow. d) Schematic of the expected differences in the vane with and without a coating for dorsal and ventral airflow. e) Experimental results plotting *f*, a quantitative measurement of the effect of barbule membranes on air capture, versus airspeed for the three species tested. An example of the barbule spacing dimension is shown in panel (f) along with SEM images that exhibit the similarities between the microscale barbules of Anna's Hummingbird (*C. anna*) (left) and the Andean Condor (*V. gryphus*) (right). g) The spacing between trailing hooked barbules ranges between 8 and 16 µm across all bird masses measured. Panels (b), (c), (f), (g): Reproduced with permission.[7] Copyright 2017, Elsevier.

coated drag force of the feather. The schematic in Figure 5d demonstrates the experiment's hypothesis. Although a very thin coating of flexible vinyl cement is used to seal feathers, there are inherent differences in stiffness between coated and uncoated feathers. These are accounted for in a normalization whereby the ratio between coated and uncoated samples due to the added stiffness of the coating is assumed to be the same for ventral and dorsal airflow. Thus one has

$$f = \frac{\text{Force}_{\text{dorsal,coated}}}{\text{Force}_{\text{dorsal,uncoated}}} \Big/ \frac{\text{Force}_{\text{ventral,coated}}}{\text{Force}_{\text{ventral,uncoated}}} \quad (2)$$

The factor f represents a normalized (accounting for the difference in stiffness introduced by coating) ratio between the dorsal and ventral drag force exerted by the feather. If $f = 1$ there is no effect of sealing barbule flaps closed, but if $f > 1$ the opening of flaps reduces the drag force. Figure 5e demonstrates that this value (f) increases with airspeed, which corroborates its meaning as a measure of the effect of the barbule membranes. With higher airspeeds, membranes are bent back more intensely, resulting in an augmented difference between coated and uncoated samples reflected in the rising value of f. Additionally, a general linear model determined that for all species the $\text{Force}_{\text{ventral,coated}}/\text{Force}_{\text{ventral,uncoated}}$ is significantly different ($P = 0.00$) from the $\text{Force}_{\text{dorsal,coated}}/\text{Force}_{\text{dorsal,uncoated}}$, further highlighting the effect of the membrane flaps on the directional permeability of the feather (see Section S5 in the Supporting Information for details).

It is proposed that flaps are designed with unidirectional permeability dependent on airflow direction because birds require more power in flight on the down/power stroke (corresponding to ventral airflow) than on the up/recovery stroke (dorsal airflow). Interestingly, at the macroscale, during the upstroke the bird's primary feathers spread apart and separate from one another to allow air-flow between them and prevent excessive downward forces on the wing.[21] Our findings suggest that the microstructural barbule flaps of wing flight feathers assist with this efficient measure.

Since the effect of membrane flaps (f) is similar for all species tested (dove, pelican, guineafowl), the spacing between barbules that is covered by these flaps is measured to determine how this scales between birds (Figure 5f,g). Despite other dimensions of the feather scaling proportionally to $\text{mass}^{1/3}$,[7,22,23] barbule spacing is found to narrowly vary between 8 and 16 µm for all birds measured, ranging from Anna's Hummingbird (*Calypte anna*) (4 g) to the Andean Condor (*Vultur gryphus*) (11 000 g)[7] (Figure 5g). Constancy in barbule spacing is proposed to be to retain low permeability of air through the feather, independent of bird size. The feather must balance air flow with maintenance of its interlocking structure.

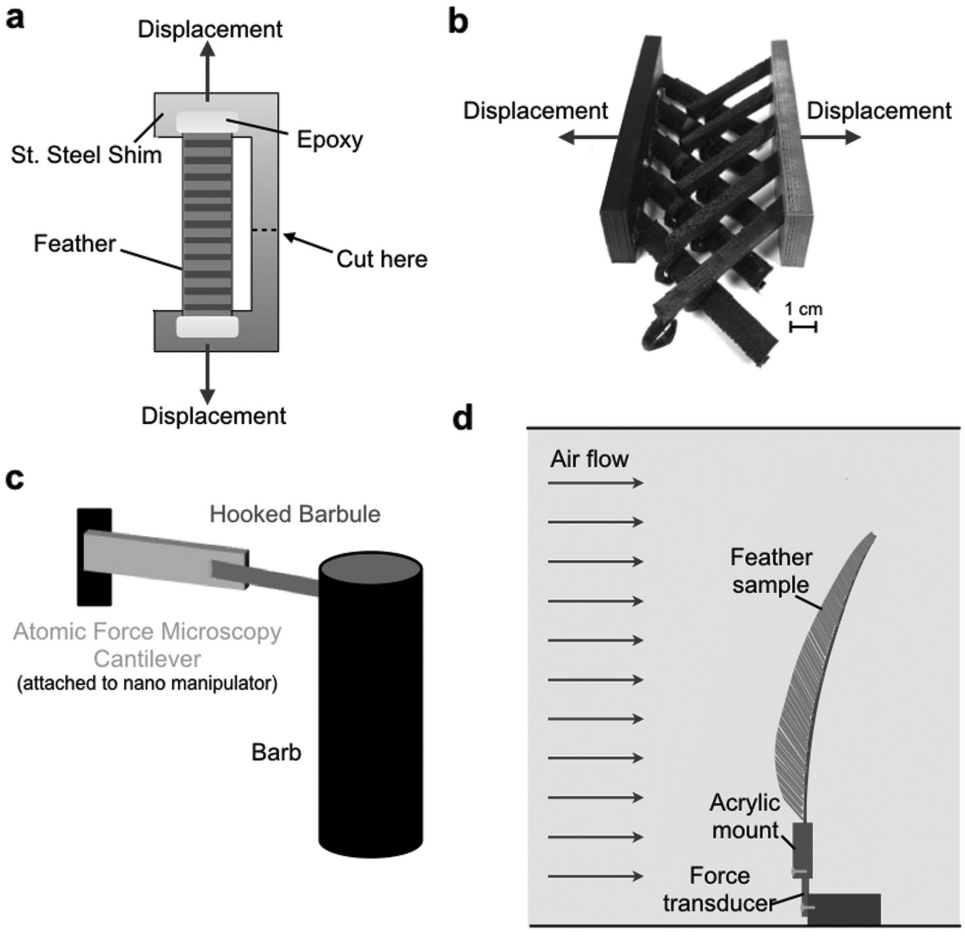

Figure 6. Schematics of various experiments: a) Experimental setup of feather-vane tension tests; the darker lines within the feather represent barbs and lighter lines barbules. b) Bioinspired interlocking barbules, with arrows showing directions of displacement in tension tests. c) Atomic force microscopy (AFM) cantilever attached to the nanomanipulator, used to displace a single hooked barbule during in situ SEM flexure tests. d) Wind tunnel experimental setup; the feather is subjected to ventral airflow.

3. Conclusions

The intricate design of the feather contributes to the unparalleled efficiency of bird flight. Here we investigate aspects of the barbule, the smallest structure in the feather, essential to the vane's function. Tests involving barbule adhesion demonstrate that the feather vane maintains in-plane tautness through contrasting directions of rotational preference at each hierarchical level. Experiments on bioinspired hook and groove barbules reveal that hooks must balance conflicting requirements for adhesion and effective readhesion, two important properties of the vane. A method for testing barbule stiffness is developed by in situ SEM experiments; this stiffness is crucial in understanding the critical failure of barbule connections. When barbules are unzipped, feathers are found to less effectively capture air; the magnitude of this effect is correlated to the barb's dimensions. Finally, the feather vane is found to have unidirectional permeability due to membranous barbule flaps that act as one-way valves and are similar in size among birds.

Barbule features examined in this paper are highly interrelated and work cooperatively with barbs to create a feather vane system that is exceptionally efficient and effective. For example, barbule stiffness and hook and groove shape influence feather vane attachment, which, along with vane permeability and barb stiffness, impacts the ability of the vane to sustain loading in flight. Barbules are exquisitely developed structures that enable impressive failure aversion combined with air capture. These multifunctional structures provide inspiration for new, more efficient aerospace materials with features such as tailored permeability and localized failure.

4. Experimental Section

Feather Samples: All feather samples used in experiments were wing flight feathers (remiges) obtained postmortem and stored in ambient conditions. Detailed information can be found in Section S6 in the Supporting Information.

Feather Vane Adhesion: The trailing vane of American White Pelican remiges were cut into rectangular pieces at ≈50% of the shaft's length and secured to a stainless steel shim using epoxy. Each of the five samples tested had a width of 4–6 mm and length of 10–20 mm. The shim was clamped in a mechanical testing device and cut in its center

just prior to testing (**Figure 6**a). Tests were carried out in tension, with displacements applied perpendicular to the length of barbs at a strain rate of 3×10^{-3} s^{-1}. Force was measured with a 250 g load cell, and displacement determined using a linear variable differential transformer. Experiments were done in situ with an optical microscope (objective of 2.5×) and images were analyzed using MATLAB (The Mathworks, Natick, MA, USA) software's image processing functions to track two rows of points at predetermined y-positions.

Adhesion of Bioinspired Hooks and Grooves: Hooks and grooves inspired by the barbules of the feather vane were drawn in SolidWorks (SolidWorks Corp., Waltham, MA, USA) and 3D printed using a MakerBot 2 Replicator (MakerBot, New York, NY, USA) (detailed information in Section S7 in the Supporting Information). In order to explore the differences in adhesion due to hook shape, five different hook shapes were created and tested with the same groove shape.

In the adhesion experiments, hooks and grooves were manually interlocked before testing and "barbs" were secured in testing grips. Tension was applied to the sample by displacing barbs apart from one another at a strain rate of 1.6×10^{-3} s^{-1} using an Instron 3342 mechanical testing machine (Instron Corp.) with a load cell of 500 N ± 0.5 N (Figure 6b). Each set of hooks was tested three times with the same set of grooves.

Hooks and grooves were then tested for their ability to readhere without external assistance (as witnessed in the feather vane). This was done by bringing hooks and grooves back to their original gauge length, and then displacing barbs apart from one another (without manually interlocking hooks and grooves) at a strain rate of 1.6×10^{-3} s^{-1}. This test was repeated three times.

Barbule Flexure Tests: The American White Pelican distal barbule's out-of-plane stiffness was measured by in situ SEM. First, barbs from the trailing edge of remiges were cut off of the rachis at 20–50% of the feather shaft length (from the base). A single barb was then isolated and secured to a SEM stub using conductive tape with the distal portion of the barb facing upward. Following this, a nanomanipulator applied a prescribed displacement via an AFM cantilever to a single hooked barbule of the barb secured on the SEM stub (Figure 6c). A digital image correlation program in MATLAB was used to determine the displacement of the hooked barbule, and the barbule stiffness was calculated (Section S3, Supporting Information). These experiments were inspired by works of Naraghi et al.[24] and Roenbeck et al.,[25] who did similar tests on inorganic materials.

Wind Tunnel Test Specimens and Setup: Wind tunnel tests were conducted on remiges from Bartlett's Bleeding Heart Dove, the American White Pelican, and the Crested Guineafowl. These three birds represent a wide variety of flying birds of various sizes, lifestyles, and flight styles. Nearly all feathers were used in their entirety during tests, the exceptions being some pelican feathers that were sliced from the base in order to properly fit in the wind tunnel.

A square wind tunnel with a height of 36 cm and a length of ≈9 m was used in experiments. The wind tunnel was calibrated to determine the airspeed for each of its programed power settings by inputting pitot tube measurements and the atmospheric air density into Bernoulli's equation. Following this, a force transducer (using load cell RB-Phi-203, 100 g ± 0.05 g) was fabricated, calibrated, and mounted inside of the wind tunnel. Feather samples were secured in an acrylic mount attached firmly to the force transducer. For each test, the center of the feather shaft was marked and aligned with the center of the acrylic mount to ensure consistent directionality during tests.

Force measurements were made at airspeeds of 0, 6.91, 10.20, 13.50, 16.80, and 20.09 m s^{-1}. This range of airspeeds covered the approximate range of speeds that the feathers encounter in actual flight. The force of the acrylic mount with no feather sample was measured at each airspeed to normalize force readings of the sample data. Images of samples were taken during the tests using a camera mounted on the exterior of the wind tunnel. Figure 6d is a schematic of the placement of the force transducer and feather samples in the wind tunnel.

Wind Tunnel—Barbule Adhesion and Air Capture: For experiments testing the effect of unzipping in the wind tunnel, feather samples were placed unaltered into the acrylic mount with their ventral side facing the airflow; the force was measured at each airspeed. Following this, feathers were taken out of the mount, unzipped using a fine-tooth comb and tweezers, placed back in the wind tunnel, and retested. This was repeated once more with a more vigorous unzipping process. Three feathers from each species were tested. Images were taken before and after each unzipping process.

Wind Tunnel—Directional Permeability of the Vane: In experiments investigating the effect of the extended membranous "flaps" of barbules on the ability of the vane to capture air, the force of unaltered feather samples was measured first in the ventral, then in the dorsal direction at each airspeed. Following this, each feather was lightly coated in SCIGRIP 66 Fast Set Flexible Vinyl Cement (SCIGRIP, Durham, NC, USA) which allowed the vane to remain flexible, yet sealed the flaps closed and prevented the vane from unzipping. After drying for at least 60 min, coated feathers were tested in the wind tunnel facing the airflow dorsally and then ventrally. The mass of feather samples was measured before and after the coating. Three feathers of each species were tested.

Fabrication of the Bioinspired Vane: The bioinspired feather vane incorporating one-way valve structures was drawn in the CAD program SolidWorks and 3D-printed using a Stratasys Objet260 Connex3 printer (Stratasys, MN, USA). Combinations of TangoBlack and VeroClear (Stratasys, MN, USA) filament were used to print each part of the feather.

Barbule Characterization: Barbules of remiges from a variety of flying birds (see Section S6 in the Supporting Information for full list of birds) with masses ranging from 4 to 11 000 g were imaged using SEM. Sections of the vane were sliced with a razor blade at 50–60% of the total shaft length, and then sonicated in ethanol for a few minutes. Following this, they were air dried, mounted to a SEM stub and imaged. The dimensions of sections of the barbules were measured using the software ImageJ (National Institutes of Health, Bethesda, MD). All feather specimens were obtained from adult birds postmortem and stored at ambient conditions.

Supporting Information

Supporting Information is available from the Wiley Online Library or from the author.

Acknowledgements

The authors graciously thank Dr. Steve Roberts (UC San Diego) for assistance with the wind tunnel. The authors also thank the San Diego Zoo (April Gorow, Research Coordinator), the San Diego Natural History Museum (Phil Unitt, Curator of Birds and Mammals), and the Los Angeles Zoo where Mike Maxcy (Curator of Birds) and Dr. Cathleen Cox (Director of Research) provided feather samples to us. Assistance with additive manufacturing by Frances Su, Profs. Joanna McKittrick and Michael Tolley is gratefully acknowledged. The authors appreciate the assistance provided by Esther Cory and Prof. Robert Sah (UC San Diego) for μ-CT scans. This work is part of the AFOSR MURI (AFOSR-FA9550-15-1-0009) and the authors thank Dr. Hugh DeLong for his support.

Conflict of Interest

The authors declare no conflict of interest.

Keywords

bioinspired design, failure aversion, feather vane, natural reversible attachment

Received: June 1, 2017
Revised: June 30, 2017
Published online:

[1] C. J. Pennycuick, *Modelling the Flying Bird*, 1st ed., Elsevier, Burlington, USA **2008**.
[2] P. R. Stettenheim, *Am. Zool.* **2000**, *40*, 461.
[3] F. B. Gill, *Ornithology*, 2nd ed., W. H. Freeman, New York, USA **1995**.
[4] L. Alibardi, *Acta Zool.* **2007**, *88*, 101.
[5] N. S. Proctor, P. J. Lynch, *Manual of Ornithology: Avian Structure & Function*, 1st ed., Yale UP, New Haven, USA **1993**.
[6] A. M. Lucas, P. R. Stettenheim, in *Avian Anatomy: Integument*, US Department of Agriculture, Washington, D.C., USA **1972**, pp. 341–419.
[7] T. N. Sullivan, B. Wang, H. D. Espinosa, M. A. Meyers, *Mater. Today* **2017**, DOI: 10.1016/j.mattod.2017.02.004.
[8] W. L. Eckalbar, S. A. Schlebusch, M. K. Mason, Z. Gill, A. V. Parker, B. M. Booker, S. Nishizaki, C. Muswamba-Nday, E. Terhune, K. Nevonen, N. Makki, *Nat. Genet.* **2016**, *48*, 5.
[9] J. Clarke, *Science* **2013**, *340*, 690.
[10] A. Kovalev, A. E. Filippov, S. N. Gorb, *J. R. Soc., Interface* **2014**, *11*, 20130988.
[11] J. Barlee, in *A New Dictionary of Birds* (Ed: A. L. Thomson), Nelson, London, UK **1964**.
[12] R. H. J. Brown, in *Biology and Comparative Physiology of Animals* (Ed: A. J. Marshall), Academic Press, New York, USA **1961**.
[13] J. J. Videler, in *Oxford Ornithology Series* (Ed: T. R. Birkhead), Oxford University Press, Oxford, UK **2005**, pp. 2–7.
[14] J. Dyck, *Zool. Scr.* **1985**, *14*, 137.
[15] A. Raspet, *Science* **1960**, *132*, 191.
[16] W. Muller, G. Patone, *J. Exp. Biol.* **1998**, *201*, 2591.
[17] A. R. Ennos, J. R. E. Hickson, A. Roberts, *J. Exp. Biol.* **1995**, *198*, 1219.
[18] B. Wang, M. A. Meyers, *Adv. Sci.* **2016**, *4*, 1600360.
[19] G. K. Batchelor, *An Introduction to Fluid Dynamics*, Cambridge University Press, Cambridge, UK **1967**.
[20] T. N. Sullivan, A. Pissarenko, S. A. Herrera, D. Kisailus, V. A. Lubarda, M. A. Meyers, *Acta Biomater.* **2016**, *41*, 27.
[21] A. Azuma, *The Biokinetics of Flying and Swimming* (Ed: J. A. Schetz), 2nd ed., American Institute of Aeronautics and Astronautics, Inc., Reston, USA **2006**.
[22] S. E. Worcester, *J. Zool.* **1996**, *239*, 609.
[23] X. Wang, R. L. Nudds, C. Palmer, G. J. Dyke, *J. Evol. Biol.* **2012**, *25*, 547.
[24] M. Naraghi, G. H. Bratzel, T. Filleter, Z. An, X. Wei, S. T. Nguyen, M. J. Buehler, H. D. Espinosa, *Adv. Funct. Mater.* **2013**, *23*, 1883.
[25] M. R. Roenbeck, A. Furmanchuk, Z. An, J. T. Paci, X. Wei, S. T. Nguyen, G. C. Schatz, H. D. Espinosa, *Nano Lett.* **2015**, *15*, 4504.

